Composite Gaussian Pulsed Waveform For Robust Resonance Radar Signature

Faisal Aldhubaib
Electronics Department, College of Technological Studies, Public Authority for Applied Education, Kuwait
Email:ff.aldhubaib@paaet.edu.kw

Abstract: The paper assesses the feasibility of forming a composite excitation pulse with a high potential to combat the noise and onset ambiguity when estimating the target resonance behaviour in a radar target signal. The assessment investigates four composite pulse configurations of unified or adaptive setups for the fractional bandwidth and peak weight to find the best setup in enhancing the resonance signature robustness. The assessment uses the method pencil function to extract the resonance parameters of the composite time data (coherent) and then determine the degree of robustness over-extraction onset and range of noise level. Determining the robustness rate requires finding the error between the original excitation frequencies and the extractable resonant frequencies and, second, the similarity between the original and reconstructed pulse waveforms. The qualitative assessments of the robustness merit concluded that the adaptive configuration of peak weight and small adaptive fractional bandwidth outperforms the other configurations in enhancing the resonance signature robustness.

Keywords—-Complex Natural Resonance, Pulsed Radar waveform, Matrix Pencil Function, Singularity Expansion Method.

1 Introduction:

A low-resolution radar system could utilize the radar target's complex natural resonance (CNR) signature in remote sensing, security or air defence applications against buried targets, concealed weapons, long-range or even low observable radar targets, respectively, e.g., [1-12]. For example, in surveillance of a wide geographic area, such proactive operation enables cueing and focusing other high-resolution radar systems on a smaller acquisition box where the potential target exists. Exciting the CNR set in the radar return requires an Ultra Wide Band signal (UWB), e.g., a Gaussian pulse of high fractional bandwidth. However, the UWB transmission and reception are subject to adverse factors like the specular content masking the resonance content at reception, transmission power restriction, low transmission average power and poor range resolution with low operating frequency.

The beforementioned factors degrade the robustness of the CNR signature in the recognition operation using techniques like Extinction pulse, e.g., [13, 14], or characteristic polarization states, e.g., [15-18]. A typical way to negate the specular masking effect is to choose a late-time start optimally that separates the specular and resonance content in the time domain or reduces the specular to resonance return by bistatic or polarization diversities. However, many researchers found that accurately selecting the onset can be daunting for unknown targets, e.g., [19-21]. For instance, delaying the onset to reduce specular contamination will likely cause extraction failure of timely localized resonances and thus poor information in the signature.

Contrary to the resonance return, the specular return is well-localized in time and well-extend in frequency, similar to the mono carrier's high fractional bandwidth pulse signal. Hence, the high fractional nature of the UWB pulse signal could incite a much higher specular return than the CNR return, especially for the normal incidence direction. In contrast, a resonance return has a smaller fractional bandwidth that extends the pulse length improving the average transmitted power; therefore, a better waveform must simultaneously manipulate the pulse fractional bandwidth and energy to decrease the specular content and elevate the resonance content in the received signal.

As a solution, therefore, the study considers modulating the Gaussian pulse by a composite of sinusoidal carriers at the resonant frequencies of interest to create resonance regions of high energy fraction, which are impacted less by adverse factors like specular return, resonance onset ambiguity or noise. Also, the modulated pulse could help reduce power restriction and increase average power and range resolution. Hence, the modulated waveform compensates for weakly excited resonances by shifting the carrier's energy towards the weaker resonance, acting as a resonator to enhance the target resonance set in the required band.

The paper hypothesizes that if the modulated Gaussian pulse improves the resonance behaviour in the excitation waveform subject to noise, the resonance set in the received radar signal will be more likely robust versus noise and onset ambiguity. A warrant that the claim that the composite Gaussian pulse with proper fractional bandwidth and peak weight can better excite the resonance set in the received radar signal than an unmodulated or mono-UWB pulse. In the proposed approach, the Matrix Pencil Function (MPOF) extracts the resonance parameters as a series of decaying exponentials, i.e., complex modes, in the Laplace domain according to the Singularity Expansion Method (SEM) model, e.g., [22, 23]. Then by applying a signal variance merit and resonant frequency error merit, the paper validates the modulated waveform robustness against degrading factors, such as time onset and noise level. The implementations of varying setups of unified or adaptive fractional bandwidth and peak weight will be

analyzed and discussed. The rest of the paper is structured as follows; section 2 presents the background, including the Gaussian pulse formulation and the SEM model; section 3 presents the methodology, including the pulse design, the robustness merit and the procedures; section 4 offers the results and discussions, including the excitation pulse characteristics and robustness performance; finally, section 5 lists the conclusions and outlines the direction of future work.

2 Background

A. Modulated Gaussian Pulse

Let us first express a double-sided gaussian pulse, in the interpulse interval $-t_c/2 \le t \le +t_c/2$, as follows

$$g(t) = \bar{a}.e^{-(1.39 f_b.f_c t)^2} \quad (1)$$

The following parameters specify the excitation pulse: carrier's centre frequency, f_c, peak amplitude, $\bar{a}$, time delay, t_d, fractional bandwidth, f_b, and the interpulse duration, t_c, —set equal $1.5/(f_b.f_c)$. Thus, decreasing the carrier's fractional bandwidth will increase the interpulse duration with more defined frequency peaks. Then a mono sinusoidal Gaussian pulse, $y(t)$, can be expressed as amplitude modulation (or multiplication) of a sinusoidal carrier at f_c by the pulse, $g(t)$, as follows:

$$y(t) = g(t)\cos(2\pi f_c t) \quad (2)$$

Figure 1 depicts the mono modulated Gaussian waveform for a 15MHz carrier given 10, 50 and 100% fractional bandwidths. The waveform decays at a higher rate with lower fractional bandwidth but will start to have a similar interpulse duration from 50% up to 100%; thus, the pulse duration is inverse proportional to the fractional bandwidth. The composite signal's cumulative (or running) sum from $\pm t$ to 0s, namely decay sum (*DS*), will assess the signal energy. Next, Figure 2 depicts the mono spectrum given three different fractional bandwidths showing that the spectrum bandwidth and power average, P_{av}, inverse the fractional bandwidth.

B. SEM Model

The SEM model a single-sided version of the mono pulse, $y_r(t \ge T_l)$, truncated at the time onset, T_l, as a single sinusoidal mode with a natural resonant frequency, ω, a negative decay factor, α, and a complex residue, r, as follows

$$y_o(t) = |r|.e^{\alpha t}\sin(\omega t + \theta_r) \quad (3)$$

Applying the MPOF to the time signal yields the estimated sinusoidal model parameters. Hence, the model can reconstruct the signal with error, ε_n, set equal to the standard deviation of $(y\text{-}y_o)$ for $t \ge T_l$.

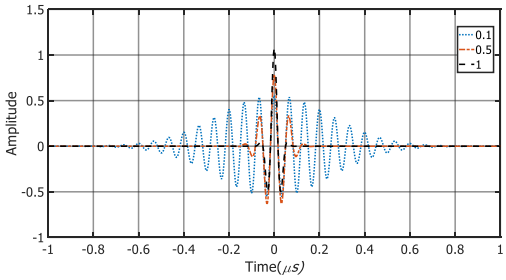

Figure 1A mono modulated Gaussian waveform per f_b=0.1, 0.5 and 1.

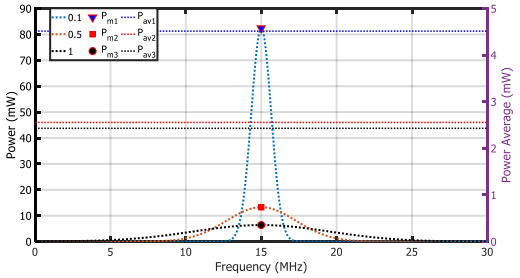

Figure 2 The mono modulated Gaussian spectrum per f_b=0.1, 0.5 and 1.

To count for the accuracy of the other model parameters, i.e., damping factor and residue, the variance amplitude figure (*VAF*) calculates the degree of resemblance between the original and reconstructed signals, y and y_o, as follows

$$VAF = (1 - \varepsilon_n/\sigma(y)) \quad (4)$$

3 Method

A. The Composite Pulse

A composite sinusoidal Gaussian pulse, $\mathbf{c}(t)$, combines several, say M, sinusoidal Gaussian pulses, ordered by the carrier frequencies (indexed from "*0*" for lowest to "*M*-1" for highest), as follows

$$\mathbf{c}(t) = c_0(t) + .. + c_{M-1}(t) \quad (5)$$

Then normalized to have unit amplitude peak at t=0, as follows

$$\bar{\mathbf{c}}(t) = \mathbf{c}(t)/\text{peak}(|\mathbf{c}(t)|) \quad (6)$$

The carriers should have half-wavelengths comparable to the target global dimensions. Then, the order of the carriers, M, must be equivalent to the number of cardinal dimensions of the target class of interest. The bandwidth is the product of the carrier frequency and fractional bandwidth; therefore, a constant bandwidth of all pulses requires that their product of carrier frequency and fractional bandwidth be kept constant. Thus, the fractional bandwidth of the m'th pulse, f_{bm}, is adaptive and determined relative to the fundamental carrier bandwidth, i.e., $f_{b0}.f_{c0}$, as follows

$$f_{bm} = f_{b0}.f_{c0}/f_{cm} \quad (7)$$

Generally, two conditions degrade the resonance strength in the received radar signal as the resonant frequency increases; or the carrier strength in the excitation signal as the fundamental fractional bandwidth increases. Therefore, an amplitude weight is applied to the *m'th* carrier to compensate for both conditions as follows

$$\bar{a}_m = k_1[(f_{cm}/f_{c0}) \times (1 + k_2.f_{b0})] \quad (8)$$

The fundamental carrier frequency, f_{c0}, is the lowest carrier frequency for the class target of interest, and now the relative amplitude of a carrier set increases with higher frequency order. The scale factor, k_1, scales down the weight set such that when k_1=0.5, the fundamental weight $\bar{a}_0$ is approximately unity for high fractional bandwidth near 100%. While the scale factor, k_2, relates the fractional bandwidth to the average power, such that, when k_2=1.15, the 10% and 100% fundamental fractional bandwidths have similar power averages except when the configuration has a unified peak weight. However, a unified peak weight setup is *M* set of $\bar{a}_0$, termed Ā, whereas a unified fractional bandwidth setup is *M* set of f_{b0}, termed F_b, such that

$$f_{bm} = f_{b0}, \bar{a}_m = \bar{a}_0 \quad (9)$$

Thus, the composite pulse can have four configurations of peak weight and fractional bandwidth as follows: (i) both unified, termed as **Ā&F$_b$**, (ii) unified fractional bandwidth only, termed as **ā&F$_b$**, (iii) unified peak weight only, termed as **Ā&f$_b$** and (iv) both adaptive, termed as **ā&f$_b$**.

B. The Rate of Robustness

The frequency's error, f_E, is the primary indicator in the time domain to assess the accuracy and consistency of the extracted carrier frequency from the single-sided composite pulse at a chosen onset time. The merit quantifies the mean squared distance between the *M* frequencies, f'_{cm} , extracted by the MPOF and the pulse assigned carrier frequencies, f_{cm}, as follows:

$$f_E = \frac{1}{M}\sum_{m=0}^{M-1} (f_{cm} - f'_{cm})^2 \quad (10)$$

A recommended constraint is that any frequency difference that exceeds the operating frequency limit should be reset equal to this limit to minimize the effect of the outlier frequency on this merit. Note that the f_E or *VAF* alone cannot reflect the robustness of the extracted resonances since the *VAF* does not account for missing resonances, whereas f_E does not account for the accuracy of the signal model. Henceforth, combining the f_E and *VAF* merits to express the rate of robustness (*RoR*) as follows

$$RoR = VAF/(1 + \sqrt{f_E})\ \% \quad (11)$$

Adding a constant in the denominator will unbias *RoR* towards a trivial error value. Thus the derived *RoR* merit is the *VAF* scaled unbiasedly by 1+f_E. Hence, a robust model extraction requires selecting fractional bandwidth and peak amplitude weight leading to minimal f_E and maximum *VAF*. Notably, determining the configuration performance requires evaluations over a time onset bin and an *SNR* bin. Thus two averages of *RoR* can be over noise at fixed onset and onset range for fixed noise level, whereas the overall or double *RoR* average is across both. Finding the overall average requires calculating the average *RoR* across the noise range for each fixed onset and its double average across the onset. A high overall *RoR* average over the onset and *SNR* bins means the configuration is more likely to be robust to the adverse factors.

C. Procedures

Table 1 shows the default simulation parameters. Given four different fractional bandwidth and peak weight configurations, the evaluation and characterization of the designed excitation signal involve deriving the following:

step 1) The values of the adaptive fractional bandwidth and carrier peak weight. (see Table 2 and Table 3)

step 2) The waveform and spectrum characteristics like peak location and power, P_m, average power, bandwidth and decay sum. (see Figure 3 to Figure 6)

step 3) The extracted resonant frequency distribution and robustness rate with onset shift (see Figure 7 to Figure 9), and the onset-average robustness rate over a chosen onset bin, ΔT_l, from 0s to T_l, when *DS* reaches 20% (see Table 4 and Table 5)

step 4) The robustness performance against noise for different extraction onsets (see Figure 10 and Figure 11, and the noise-average robustness rate over +20:20dB noise levels. (see Table 6)

step 5) The performance of the overall robustness average across noise and onset delay. (see Table 7)

Table 1. The simulation parameters,

Symbol	Name	Value
f	Frequency limits	0-30MHz
t_c	Interpulse duration (default *D*=1.5)	D/(f_c.f_b)
N_t	no. of samples	1024
Δt	Sampling Time	tc/N_t
f_b	Fractional bandwidth	0.1-1
f_c	carrier frequency	9, 14, 24MHz
σ_n	Noise power range	-20 to 20dBW

M	Model order	3

4 Results and Discussions:

Let us set the carrier frequencies based on the fundamental resonance frequencies of a midsized aircraft, like F16, which are at 9, 14 and 24MHz. Hence, the default composite modulated pulse has three sinusoidal carriers at 9, 14 and 24MHz with an adaptive peak weight set derived in Table 2. The fundamental fractional bandwidth, $f_{b0,}$ can range from 10 to 100% with an adaptive fractional bandwidth set, derived in Table 3.

Table 2. The adaptive peak weight per fractional bandwidth with k_1=0.5 and k_2=1.15. (rounded to two digits)

f_{b0}	**0.10**	**0.20**	**0.30**	**0.40**	**0.50**
a_0	*0.56*	*0.62*	*0.67*	*0.73*	*0.79*
a_1	*0.87*	*0.96*	*1.05*	*1.14*	*1.23*
a_2	*1.49*	*1.64*	*1.79*	*1.95*	*2.10*
f_{b0}	**0.60**	**0.70**	**0.80**	**0.90**	**1.00**
a_0	*0.85*	*0.90*	*0.96*	*1.02*	*1.08*
a_1	*1.31*	*1.40*	*1.49*	*1.58*	*1.67*
a_2	*2.25*	*2.41*	*2.56*	*2.71*	*2.87*

Table 3. The fundamental and m'th fractional bandwidths.

f_{b0}	**0.10**	**0.20**	**0.30**	**0.40**	**0.50**
f_{b1}	*0.06*	*0.13*	*0.19*	*0.26*	*0.32*
f_{b2}	*0.04*	*0.08*	*0.11*	*0.15*	*0.19*
f_{b0}	**0.60**	**0.70**	**0.80**	**0.90**	**1.00**
f_{b1}	*0.39*	*0.45*	*0.51*	*0.58*	*0.64*
f_{b2}	*0.23*	*0.26*	*0.30*	*0.34*	*0.38*

A. Pulse Characteristics

The pulse design results present the single-sided waveform (with decaying sum shown as inset) for f_{b0}=10% per configuration in Figure 3, and the fourth configuration based waveforms per fractional bandwidth, f_{b0}=10, 30, 50 and 70%, in Figure 4. All configuration for f_{b0}=10% shows that the waveform amplitude converges to zero near t=1μs but at different decay rates, such that the unified fractional bandwidth, i.e., second then first configurations, have the fastest decay rates.

Hence, the first and second configurations based waveforms converge to *DS*=20% between 0.2 and 0.3μs, whereas the third and fourth configurations at around t=0.4μs, verifying that the decay rate is lower with adaptive fractional bandwidth setup. The higher fractional bandwidth compresses the waveform; for example, for f_{b0}=50 and 70%, the waveforms converge to the *DS*=20% threshold before t=0.1μs, respectively, as seen in Figure 4 inset. A small change in f_{b0}=10 to 30% led to a considerable shift in the onset of the *DS*=20% threshold from near t=0.4 to 0.125μs for f_{b0}=30%.

Next, with each carrier's power average indicated and peak location marked down to 5% of their respective maximum, Figure 5 shows samples of spectrums for the first and second configurations, i.e., unified fractional bandwidth. Illustrating that second and third carrier peaks of sizeable fractional bandwidth, e.g., f_{b0}=100%, are much less distinguishable or defined; for example, the first and the second carrier peaks seem to merge into one peak.

Using an adaptive weight setup only improves the power average for sizeable fractional bandwidth, such as P_{av}=16mW for unified weight setup to near 40mW for adaptive weight setup. Furthermore, Figure 6 illustrates the third and fourth configurations, i.e., adaptive fractional bandwidth, depicting distinguishable carrier peaks emerging in all configurations, especially the third carrier as its peak power reaches its highest level with the fourth configuration slightly above the 60mW level (see Figure 6(*b*)). However, minimizing the power gap due to the sizeable f_{b0} requires applying an adaptive peak weight setup, as seen by the similar power averages near 40mW and 57mW for f_{b0}=10 and 100% in Figure 5(*b*) and Figure 6(*b*), respectively.

B. Robustness Performance

For the four configurations of peak weight and fractional bandwidth, Figure 7 and Figure 8 illustrate the robustness rate of the extracted sinusoidal carriers given f_{b0}=10%, showing the extracted frequency distribution with the extraction onset shift, followed by Figure 9 for adaptive weight and fractional bandwidth with f_{b0}=50 and 100%. The extraction with onset shift begins at T_l=0s, i.e. *DS*=100%, and stops at the onset time when *DS* reaches 20%, at about T_l=275 and 400ns given f_{b0}=10% for unified and adaptive weights, respectively.

In Figure 7 and Figure 8, when f_{b0}=10%, all configurations lead to robust extraction as their *RoR* averages are constantly above 95%, except the first configuration underperforming as it has accumulated relatively lower average *RoR* over the onset bin ΔT_l=200-250ns. Also, the frequency error is always trivial across the onset bin except for the small error over the onset bin ΔT_l=200-250ns for the first configuration.

In Figure 9, the extraction of the *RoR* average drops for f_{b0}=50 and 100%, making the performance inferior with sizeable fractional bandwidth. The frequency error contribution for f_{b0}=100% is mainly due to the third than the second carrier.

Table 4 summarizes the average robustness performance, over the onset bin, of the four configurations per the fractional bandwidth set, f_{b0}=0.1, 0.3, 0.5, 0.7 and 0.9, at 100dB. On average, the third configuration outperforms the rest, but only at f_{b0}=*0.1*

do the configurations, except the first, perform similarly.

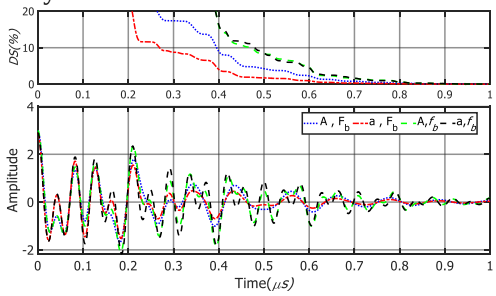

Figure 3 The waveforms and decay sum (inset) for f_{b0} =0.1 per configuration.($\bar{a}$ & f_b (black solid) $\bar{A}$ & f_b (green dashed dot) $\bar{A}$ & F_b ,(blue dotted) $\bar{a}$ & F_b (red dash-dotted))

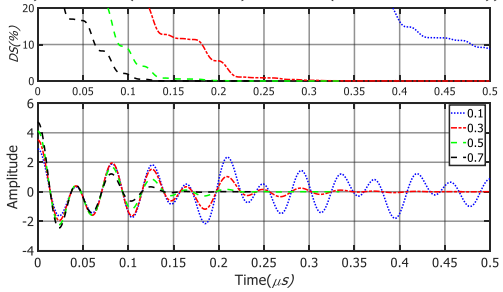

Figure 4 The waveforms per fractional bandwidth, f_{b0}(as legend shows) for the fourth configuration ($\bar{a}$ &f_b).

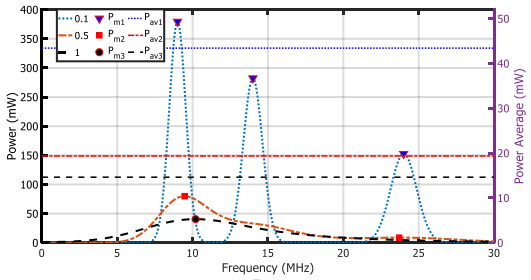

(a) $\bar{A}$ &F_b

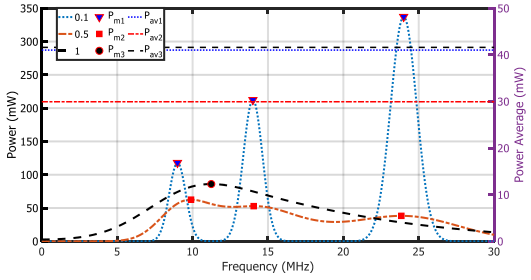

(b) $\bar{a}$ &F_b

Figure 5 The spectrums per, f_{b0}, for (a) first and (b) second configurations. (right axis: horizontal dotted lines represent the power average per f_{b0})

Table 4. The RoR average over onset bin at 100dB

f_{b0}	0.1	0.3	0.5	0.7	0.9	Mean
$\bar{A}$ &F_b	*87.3*	*62.7*	*50.1*	*29.9*	*15.9*	**49.2**
$\bar{a}$ &F_b	*96.1*	*81.5*	*40.8*	*25.7*	*18.8*	**52.6**
$\bar{A}$ &f_b	*98.4*	*91.5*	*63.4*	*37.5*	*32.8*	**64.7**
$\bar{a}$ &f_b	*98.1*	*84.4*	*61.2*	*31.1*	*27.8*	**60.5**

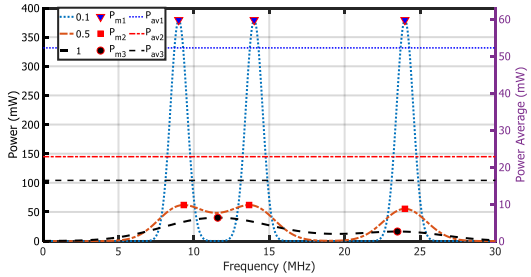

(b) $\bar{A}$ &f_b

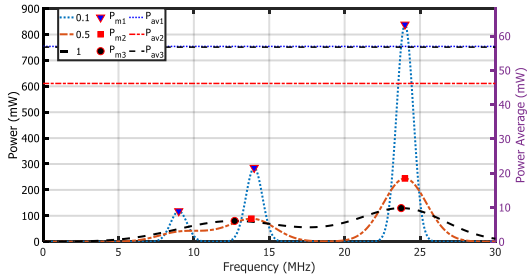

(b) $\bar{a}$ &f_b

Figure 6 The spectrums per fractional bandwidth for (a) third and (b) fourth configurations.

However, Table 5 predicts that the fourth configuration outperforms others when *SNR*=0dB. For two cases of fractional bandwidth, f_{b0}=0.3 and 0.6 at T_l=0μs and averaged over ten trials, Figure 10 displays per configuration the robustness performance versus the noise level +20:-20dB, i.e., signal-to-noise ratio (*SNR*) of -20:+20dB, assuming that the pulse power is 0dBW. The configurations have good *RoR* when f_{b0} is low and *SNR* is high, with the third and fourth configurations performing best. Nevertheless, as f_{b0} increases or *SNR* drops, the first two unified weight configurations' performance worsens faster, whereas adaptive fractional bandwidth configurations perform better above 0dB for f_{b0}=0.6.

The third configuration has the highest *RoR* averages over noise when f_{b0}=30 and 60%, respectively. With f_{b0}=10%, Figure 11 shows that the *RoR* performance worsens with onset delay, significantly faster for the unified weight setups. The adaptive fractional bandwidth setups have an *RoR* above 60% at 0dB for all selected onsets. The fourth configuration slightly outperforms the third for T_l=0s, but the third begins to outperform with delay.

Table 5. The RoR average over onset bin at 10dB

f_{b0}	0.1	0.3	0.5	0.7	0.9	Mean
$\bar{A}$ &F_b	*36.7*	*16.1*	*4.6*	*4.3*	*5.0*	**13.3**
$\bar{a}$ &F_b	*49.1*	*23.8*	*5.6*	*6.0*	*6.5*	**18.2**
$\bar{A}$ &f_b	*71.9*	*43.6*	*22.4*	*5.8*	*5.5*	**29.8**
$\bar{a}$ &f_b	*75.3*	*44.5*	*23.3*	*12.3*	*7.8*	**32.6**

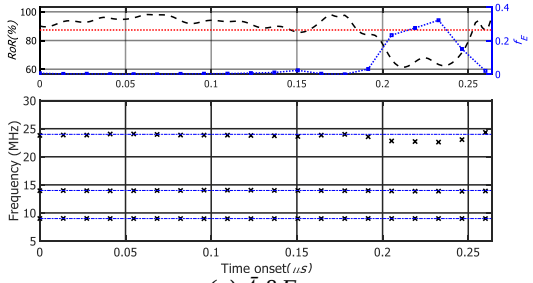

(a) $\bar{A}$ &F_b

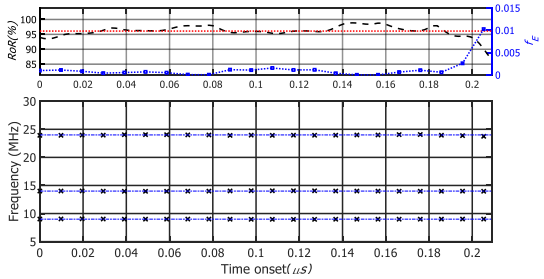

(b) $\bar{a}$ &F_b

Figure 7 The extracted carrier frequencies (marked 'x') with ime onset for first and second configurations given f_{b0}=0.1. (inset: left axis- the RoR curve (dashed-dot)and mean line (horizontal red dotted), right axis- the f_E curve(blue dotted,marked '□'))

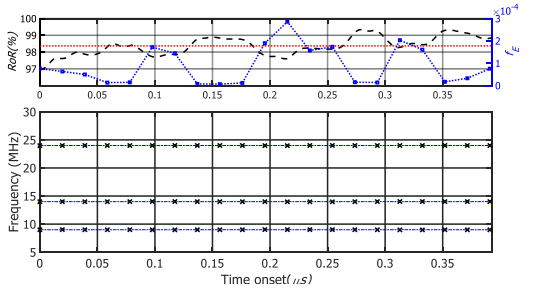

(b) $\bar{A}$ &f_b

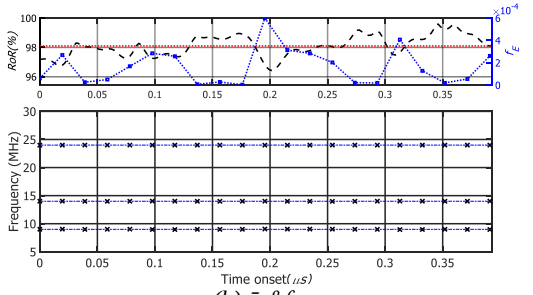

(b) $\bar{a}$ &f_b

Figure 8 The extracted carrier frequencies as a function of time onset for third and fourth configurations with f_{b0}=0.1.

Table 6 summarizes the performance of the average robustness rate over the noise range (*SNR*=-20:20 dB) for the four configurations per fractional bandwidth f_{b0}=0.1,0.3,0.5,0.7 and 0.9. The result confirms that the fourth configuration mean, across f_b, outperforms the rest in combating the noise. Finally, Table 7 shows that the fourth configuration slightly outperforms the third in terms of the overall performance against the noise and onset delay factors.

Table 6. The RoR average over noise range -20 to 20dB at T_l=0s.

f_{b0}	0.1	0.3	0.5	0.7	0.9	Mean
$\bar{A}$ &F_b	*60.7*	*39.4*	*14.1*	*10.4*	*10.5*	**27.0**
$\bar{a}$ &F_b	*61.6*	*46.7*	*15.9*	*11.7*	*12.3*	**29.7**
$\bar{A}$ &f_b	*71.3*	*53.4*	*25.5*	*16.3*	*13.0*	**35.9**
$\bar{a}$ &f_b	*69.4*	*55.3*	*29.1*	*18.1*	*17.0*	**37.8**

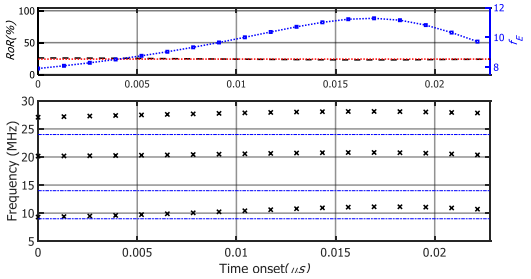

(a)

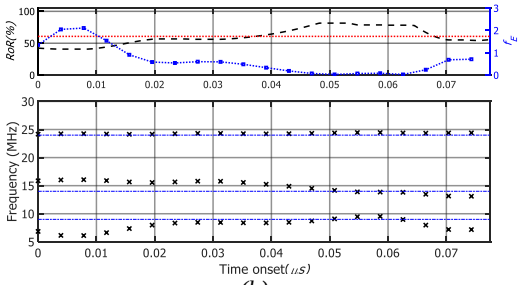

(b)

Figure 9 The extracted carrier frequencies as a function of time onset for the fourth configuration given that f_{b0}= (a) 1, (b)0.5.

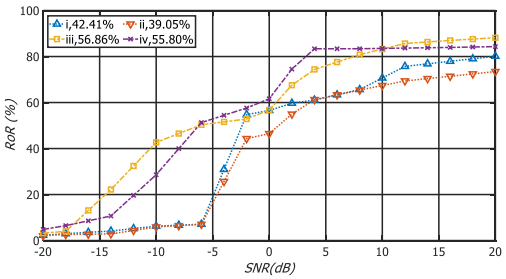

(a)

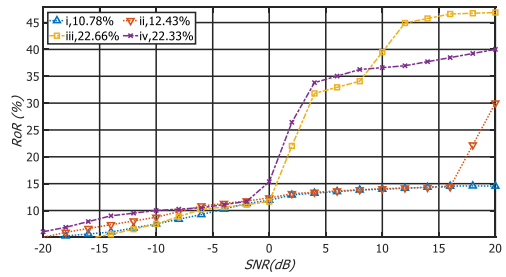

(b)

Figure 10 The robustness performance (per configuration) at T_l=0μs given f_{b0} = (a)0.3 and (b)0.6.

Table 7. The overall RoR average over noise and onset bin.

f_{b0}	0.1	0.3	0.5	0.7	0.9	Mean
$\bar{A}$ &F_b	*11.7*	*8.7*	*7.5*	*7.5*	*7.5*	**8.6**
$\bar{a}$ &F_b	*12.2*	*9.3*	*7.9*	*8.0*	*8.0*	**9.1**
$\bar{A}$ &f_b	*24.1*	*20.7*	*17.6*	*15.3*	*14.6*	**18.4**
$\bar{a}$ &f_b	*24.5*	*21.7*	*18.2*	*16.3*	*15.9*	**19.3**

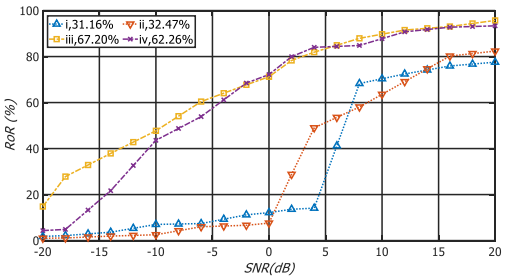

(a)

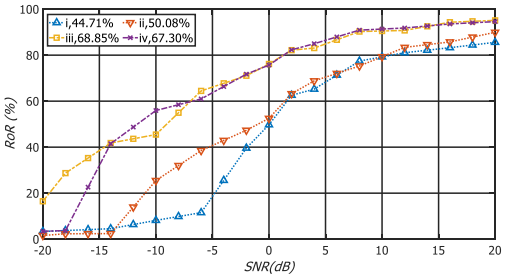

(b)

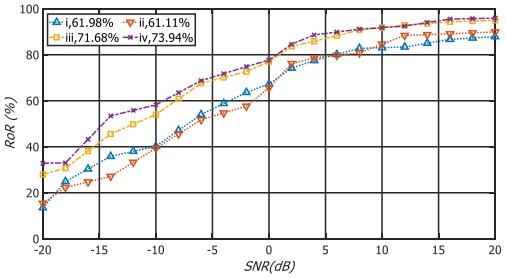

(c)

Figure 11 The robustness performance for f_{b0}=0.1(per configuration) at T_l= (a) 0.2μs, (b) 0.1μs and (c)0μs.

5 Conclusions:

In a unified fractional setup with high fractional bandwidth, the first and second configurations had less distinguishable or defined second and third carrier peaks in the frequency domain. An adaptive weight setup only improved the power average for sizeable fractional bandwidth. Furthermore, an adaptive fractional bandwidth setup spectrum had distinguishable carrier peaks, especially the third carrier, as its peak power reaches its highest level with the fourth configuration. However, minimizing the power gap due to the sizeable fractional bandwidth required applying an adaptive peak weight setup.

All configurations yielded robust extraction at high *SNR* with a small fractional bandwidth, i.e., f_{b0}=0.1, except the first underperforming configuration. The frequency error was always trivial across the onset bin except for the first configuration. The robustness average over the onset bin at high *SNR* showed that the third configuration outperforms the rest, but only at f_{b0}=*0.1* do the configurations, except the first, perform similarly. However, when *SNR*=0dB, the fourth configuration outperform the third. As fractional bandwidth increases or noise highs, the first two unified weight configurations' performance worsens faster. The robustness performance worsens with onset delay, significantly faster for the unified weight setups. The fourth configuration slightly outperforms the third with no onset delay, but the third outperformed when more delay or noise was introduced. The overall robustness rate average over the noise range and time delay confirmed that the fourth configuration outperforms the rest in combating the noise and onset delay factors.

Future work should assess the ability of composite excitation pulse to improve the resonance signature of the radar target return with diversification in aspect and polarization directions.

Acknowledgement: This work was supported and funded by The Public Authority of Education and Training, Research Project No (TS-**-**).

References

[1] J. E. Mooney, Z. Ding, and L. S. Riggs, "Performance analysis of an automated E-pulse target discrimination scheme," Antennas and Propagation, IEEE Transactions on, vol. 48, no. 4, pp. 619-628, 2000.

[2] H. S. Lui and N. V. Z. Shuley, "Radar Target Identification Using a "Banded" E-pulse Technique," Antennas and Propagation, IEEE Transactions on, vol. 54, no. 12, pp. 3874-3881, 2006.

[3] D. Blanco, D. P. Ruiz, E. Alameda, and M. C. Carrion, "An asymptotically unbiased E-pulse-based scheme for radar target discrimination," Antennas and Propagation, IEEE Transactions on, vol. 52, no. 5, pp. 1348-1350, 2004.

[4] Q. Li, P. Ilavarasan, J. E. Ross, E. J. Rothwell, K.-M. Chen, and D. P. Nyquist, "Radar target identification using a combined early-time/late-time E-pulse technique," Antennas and Propagation, IEEE Transactions on, vol. 46, no. 9, pp. 1272-1278, 1998.

[5] J. D. Morales, D. Blanco, D. P. Ruiz, and M. C. Carrion, "Radar-Target Identification via Exponential Extinction-Pulse Synthesis," Antennas and Propagation, IEEE Transactions on, vol. 55, no. 7, pp. 2064-2072, 2007.

[6] J. H. Lee and H. T. Kim, "Radar Target Discrimination Using Transient Response Reconstruction," Journal of Electromagnetic Waves and Applications, vol. 19, no. 5, pp. 655-669, 2005/01/01 2005, doi: 10.1163/1569393053305062.

[7] J. H. Lee and S. H. Jeong, "Performance of natural frequency-based target detection in frequency domain," Journal of Electromagnetic Waves and Applications, vol. 26, no. 17-18, pp. 2426-2437,

2012/12/01 2012, doi: 10.1080/09205071.2012.735789.
[8] I.-H. Kim, I.-S. Choi, and D.-Y. Chae, "A Study on the Performance Enhancement of Radar Target Classification Using the Two-Level Feature Vector Fusion Method," J Electromagn Eng Sci, vol. 18, no. 3, pp. 206-211, 7 2018, doi: 10.26866/jees.2018.18.3.206.
[9] S.-J. Lee, I.-S. Choi, and D.-Y. Chae, "A novel feature extraction method for radar target classification using fusion of early-time and late-time regions," Journal of Electromagnetic Waves and Applications, vol. 31, no. 10, pp. 1020-1033, 2017/07/03 2017, doi: 10.1080/09205071.2017.1324324.
[10] F. Aldhubaib, "Generic aircraft model recognition by two shape factors: in the resonance region," IET Radar, Sonar & Navigation, vol. 14, no. 1, pp. 81-88, 2020, doi: 10.1049/iet-rsn.2019.0089.
[11] F. Aldhubaib, "Binary Stokes vector representation of aircraft in the low-resolution radar context," IET Radar, Sonar &Navigation, vol. 13, no. 11, pp. 2041-2045.
[12] F. Aldhubaib and N. V. Shuley, "Radar Target Recognition Based on Modified Characteristic Polarization States," IEEE Transactions on Aerospace and Electronic Systems, vol. 46, no. 4, pp. 1921-1933, 2010, doi: 10.1109/TAES.2010.5595604.
[13] H. H. Abdullah, A. B. Musa, T. G. Abulnaga, and H. Elsadek, "Practical Implementation of the E-Pulse Technique on the Original Antiquates," in 2018 Progress in Electromagnetics Research Symposium (PIERS-Toyama), 1-4 Aug. 2018 2018, pp. 1194-1197, doi: 10.23919/PIERS.2018.8597677.
[14] H. S. Lui, F. Aldhubaib, N. V. Shuley, and M. Persson, "Performance analysis of resonance based radar target recognition with different excitation bandwidth using the E-Pulse technique," in Radar Conference, 2009. EuRAD 2009. European, Sept. 30 2009-Oct. 2 2009 2009, pp. 469-472.
[15] F. Aldhubaib, H. S. Lui, N. V. Shuley, and A. Al-Zayed, "Aspect segmentation and feature selection of radar targets based on average probability of error," IET Microwaves, Antennas & Propagation, vol. 4, no. 10, pp. 1654-1664, 2010.
[16] F. F. H. Aldhubaib and N. V. Z. Shuley, "Characteristic Polarization States Estimation in an Ultrawideband Context: A Frequency Approach," IEEE Transactions on Geoscience and Remote Sensing, vol. 47, no. 8, pp. 2808-2817, 2009, doi: 10.1109/TGRS.2009.2014564.
[17] F. Aldhubaib, N. V. Shuley, and H. S. Lui, "Characteristic Polarization States in an Ultrawideband Context Based on the Singularity Expansion Method," IEEE Geoscience and Remote Sensing Letters, vol. 6, no. 4, pp. 792-796, 2009, doi: 10.1109/LGRS.2009.2025611.
[18] H. S. Lui and N. V. Shuley, "Resonance Based Target Recognition Using Ultrawideband Polarimetric Signatures," IEEE Transactions on Antennas and Propagation, vol. 60, no. 8, pp. 3985-3988, 2012, doi: 10.1109/TAP.2012.2201074.
[19] F. Aldhubaib, "Enhancing the SEM Signature via the Optimum Onset with a Bistatic and Cross-polarization Radar Configuration," IEEE ACCESS, no. 8, 2020.
[20] F. Aldhubaib, "Impact of Onset Ambiguity on SEM Signature and Reduction Approach by Scattering and Polarization Diversification," Journal of Electromagnetic Analysis and Applications, vol. 12, no. 3, pp. 29-42, 2020.
[21] C. O. Hargrave, I. V. L. Clarkson, and H. Lui, "Late-Time Estimation for Resonance-Based Radar Target Identification," IEEE Transactions on Antennas and Propagation, vol. 62, no. 11, pp. 5865-5871, 2014, doi: 10.1109/TAP.2014.2350507.
[22] T. K. Sarkar and O. Pereira, "Using the matrix pencil method to estimate the parameters of a sum of complex exponentials," Antennas and Propagation Magazine, IEEE, vol. 37, no. 1, pp. 48-55, 1995.
[23] M. Khodjet-Kesba, K. E. K. Drissi, S. Lee, K. Kerroum, C. Faure, and C. Pasquier, "Comparison of Matrix Pencil Extracted Features in Time Domain and in Frequency Domain for Radar Target Classification," International Journal of Antennas and Propagation, vol. 2014, p. 9, 2014, Art no. 930581, doi: 10.1155/2014/930581.

Faisal Aldhubaib (Electronics Department, College of Technological Studies, Public Authority for Applied Education, Kuwait)
Email: ff.aldhubaib@paaet.edu.kw